Lawrence Berkeley Laboratory

UNIVERSITY OF CALIFORNIA

Recent Results from NA35 Collaboration at CERN

NA35 Collaboration

December 1988

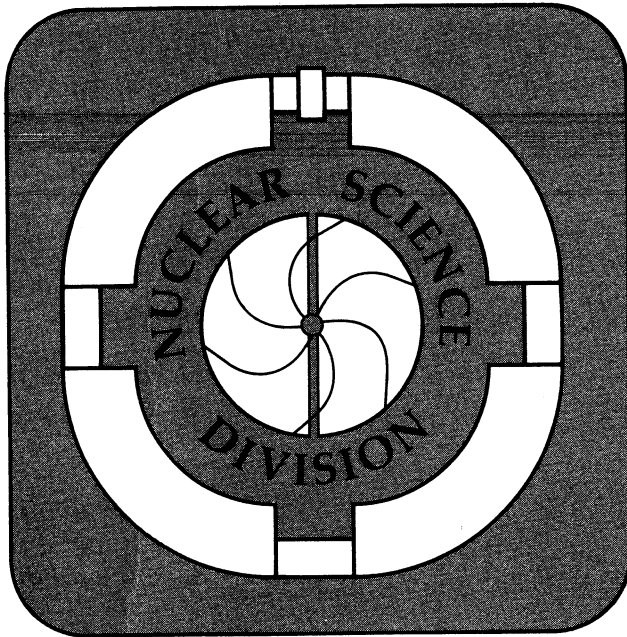# RECENT RESULTS FROM THE NA35 COLLABORATION AT CERN

John W. HARRIS

Nuclear Science Division, Lawrence Berkeley Laboratory,
1 Cyclotron Road, Berkeley, CA 94720, USA

NA35 Collaboration
A. Bamberger,[1] D. Bangert,[2] J. Bartke,[3] H. Bialkowska,[4] R. Bock,[5] R. Brockmann,[5] S.I. Chase,[6]
C. De Marzo,[7] M. De Palma,[7] I. Derado,[8] V. Eckardt,[8] C. Favuzzi,[7] J. Fendt,[8] D. Ferenc,[9]
H. Fessler,[8] P. Freund,[8] M. Gazdzicki,[10] H.J. Gebauer,[8] K. Geissler,[2] E. Gladysz,[3] C. Guerra,[5]
J.W. Harris,[6] W. Heck,[11] T. Humanic,[5] K. Kadija,[8,9] A. Karabarbounis, [12] R. Keidel,[13]
J. Kosiec,[14] M. Kowalski,[3] S. Margetis, [11] E. Nappi,[7] G. Odyniec,[6] G. Paic,[9] A. Panagiotou,[12]
A. Petridis,[12] J. Pfennig,[11] F. Posa,[7] K.P. Pretzl,[8] H.G. Pugh,[6] F. Pühlhofer,[13] G. Rai,[6]
A. Ranieri,[7] W. Rauch,[6] R. Renfordt,[11] D. Röhrich,[11] K. Runge,[1] A. Sandoval,[5] D. Schall,[10]
N. Schmitz,[8] L.S. Schroeder,[6] G. Selvaggi,[7] P. Seyboth,[8] J. Seyerlein,[8] E. Skrzypczak,[14]
P. Spinelli, [7] R. Stock,[2,11] H. Ströbele,[11] A. Thomas,[11] M. Tincknell,[6] L. Teitelbaum,[6]
S. Tonse,[6] G. Vesztergombi,[8] D. Vranic,[9] and S. Wenig[11]

[1]Fakultät für Physik, Universität Freiburg, D-7800 Freiburg, Germany
[2]CERN, CH-1211 Geneva 23, Switzerland
[3]Institute of Nuclear Physics, PL-30055 Cracow, Poland
[4]Institute of Nuclear Studies, PL-00681 Warszawa, Poland
[5]Gesellschaft für Schwerionenforschung, D-6100 Darmstadt 11, Germany
[6]Lawrence Berkeley Laboratory, University of California, Berkeley CA 94720, USA
[7]Dipartimento di Fisica, Universita di Bari, and INFN, I-70126 Bari Italy
[8]Max-Planck-Institut für Physik und Astrophysik, D-8000 München, Germany
[9]Rudjer Boskovic Institute, 41001 Zagreb, Yugoslavia
[10]Institut für Hochenergiephysik, Universität Heidelberg, D-6900 Heidelberg, Germany
[11]Fachbereich Physik, Universität Frankfurt, D-6000 Frankfurt, Germany
[12]Physics Department, University of Athens, GR-157-71 Athens, Greece
[13]Fachbereich Physik, Universität Marburg, D-3550 Marburg, Germany
[14]Institute of Experimental Physics, University of Warsaw, PL-00681 Warszawa, Poland
[a]On leave of absence from Central Research Institute for Physics, Budapest, Hungary

Recent results from the NA35 Collaboration are presented for the reactions of 60 and
200 GeV/nucleon p and ^{16}O, and 200 GeV/nucleon ^{32}S with various targets ranging from
S to Au. Midrapidity transverse energy distributions and forward energy flow, $p_\perp$ spectra
and rapidity distributions of hadrons are presented. Two-pion interferometry results are
discussed. Neutral strange particle yields and $p_\perp$ distributions are presented. Conclusions
are drawn from the experimental results.

1. INTRODUCTION

While possible formation of a quark-gluon plasma is the underlying motivation for this field
of physics, a study of the dynamics of the collision processes is of fundamental importance to
understanding the microscopic structure of hadronic interactions at high densities and the condi-
tions for formation of the plasma. In the following report, highlights of recent results from the
NA35 Collaboration will be presented. The NA35 experiment will briefly be described, along with
the physical observables accessible in the experiment. Transverse energy distributions and their
relevence to the degree of nuclear stopping in these collisions will be presented. The primary

emphasis of this experiment is the study of hadron production in high energy nucleus-nucleus collisions, where rapidity and transverse momentum distributions of hadrons provide information on the dynamics of the collision processes. Pion interferometry measurements yield insight into the space-time evolution of the reaction and possibly the existence of a quark-gluon plasma phase. The abundances of strange particles produced in these collisions can be compared to predictions of models based on flavor equilibrium in a plasma phase. All of this information will contribute to the understanding of hadronic interactions at high densities and the dynamics of high energy nucleus-nucleus reactions, whose understanding is seminal in the determination of whether or not a quark-gluon plasma is formed.

2. EXPERIMENTAL SETUP AND PHYSICAL OBSERVABLES

In this experiment 60 and 200 GeV/nucleon p, ^{16}O and 200 GeV/nucleon ^{32}S beams incident on nuclear targets varying in mass from S to Au were studied. The experiment consisted of a 2 x 1.4 x 0.7 m^3 Streamer Chamber in a 1.5 Tesla Vertex magnet, followed downstream by combined electromagnetic and hadronic calorimeters.[1] These consist of the "Veto" calorimeter, measuring the leading energy in the projectile fragmentation region ($0° < \theta_{lab} < 0.3°$), a moderate granularity "Ring" calorimeter and high granularity "PPD" electromagnetic calorimeter, measuring the transverse energy in the midrapidity region ($2.3° < \theta_{lab} < 12.5°$), and an "Intermediate" calorimeter in the region $.3° < \theta_{lab} < 2.3°$. The Streamer Chamber was read out by two independent optical systems: a set of three 70 mm film cameras, each with a high gain 90 mm image intensifier; and a set of three image-intensified charge-coupled device cameras,[2] each with one million picture elements and 9-bit intensity resolution. The Streamer Chamber provides a measure of the multiplicity of charged-particles and their pseudorapidity (η), rigidity (momentum/charge) and curvature (charge sign). Neutral strange particles were identified by their charged decay products providing a measure of the average abundance of strangeness in the final state. Transverse momentum ($p_\perp$) and pseudorapidity (η) distributions of positively- and negatively-charged particles can be measured. Two-particle interferometry measurements can be made to determine the size of the emitting source at the time interactions cease (freezeout).

3. TRANSVERSE ENERGY DISTRIBUTIONS

A systematic study of transverse energy ($E_\perp$) production at midrapidity and energy flow in the forward direction for 60 and 200 GeV/nucleon ^{16}O-induced interactions from the NA35 Collaboration has been published.[3,4] One conclusion from that study was that sufficient stopping occurs in small impact parameter collisions of ^{16}O incident on heavy targets at these energies to produce energy densities of $\epsilon \approx$ 2-3 GeV/fm^3. Additional measurements utilising a ^{32}S beam at 200 GeV/nucleon have since been completed and analysed. These are displayed in Fig. 1 in terms of a correlation between $E_\perp$ detected in the region $2.2 < \eta < 3.6$ and the energy (E_{VETO}) measured in the forward $0° < \theta < 0.3°$ ($\eta > 5.95$) fragmentation region for each of four target nuclei used. There is a distinct anticorrelation between $E_\perp$ and E_{VETO} as expected. In peripheral collisions

where values of E_{VETO} are near the total energy of the incident ^{32}S beam (6.4 TeV) there is little $E_\perp$ produced. At lower values of E_{VETO}, corresponding in a geometrical model to smaller impact parameters, $< E_\perp >$ increases. For S + S interactions few events are observed for E_{VETO} values near zero, whereas the data extend down to $E_{VETO} = 0$ for the most central S + Au interactions. Thus, for the heaviest targets and the most central collisions all of the incident longitudinal energy of the projectile has been transformed into transverse degrees of freedom, away from the fragmentation region, leaving $E_{VETO} = 0$. For S + S interactions there is always some energy remaining in the projectile fragmentation region, even in the most central collisions, due to noninteracting nucleons in the dilute corona of the interacting nuclei.
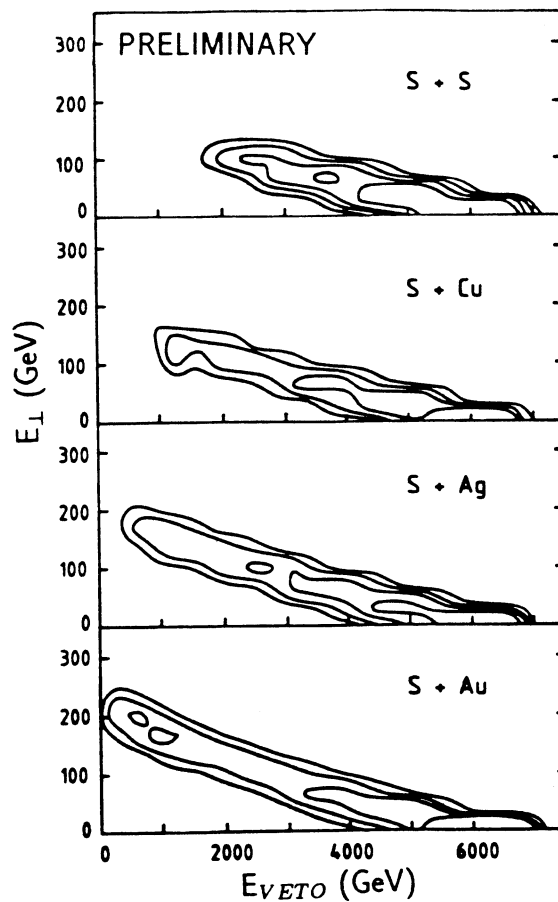

Figure 1. Contour plots of constant cross section as a function of transverse energy $E_\perp$ detected in the region $2.2 < \eta < 3.6$ and energy E_{VETO} measured in the forward $0° < \theta < 0.3°$ $(\eta > 5.95)$ fragmentation region for reactions of 200 GeV/n S incident on various targets for a minimum bias trigger.

Displayed in Fig. 2 are the $E_\perp$ distributions for 200 GeV/nucleon S + S, Cu, RbBr, Ag and Au. These $E_\perp$ distributions have the characteristic shape[3] described by a geometrical convolution of $E_\perp$ distributions for the impact parameters incident in the interaction. The "tail", or high $E_\perp$ end, of the $E_\perp$ distribution extends to larger values of $E_\perp$ for higher mass targets. If $E_\perp^{max}$ is defined as the maximum transverse energy possible in 4π solid angle, assuming all the energy is emitted isotropically in the center-of-mass of the participants, then there exists an approximate scaling of

the distributions of Fig. 2 when plotted as a function of $E_\perp/E_\perp^{max}$ for the various targets. This was observed for the case of O + Au.[4] Comparing the $E_\perp$ distributions for 200 GeV/nucleon ^{16}O + Au and ^{32}S + Au, the extreme values of $E_\perp$ on the tails of the distributions are identical when the ^{16}O + Au distribution is scaled by the factor $E_\perp^{max}(S)$ / $E_\perp^{max}(O)$ = 1.77. This is observed in Fig. 3. This value is close to the expected geometrical dependence in the high energy limit,[5] $E_\perp^{max} \sim A_P^{5/6} A_T^{1/6}$. However, the slope of the "tail" falls off more rapidly for the heavier projectile than for the lighter one. The shoulder near the end of the plateau, commonly known as the central collision peak, appears to scale with a value larger than 1.77, approximately 2. Therefore, these observations do not preclude an explanation of the ^{32}S + Au central collision data in terms of a convolution of p + Au interactions which was successful in describing the ^{16}O + Au data.[3]
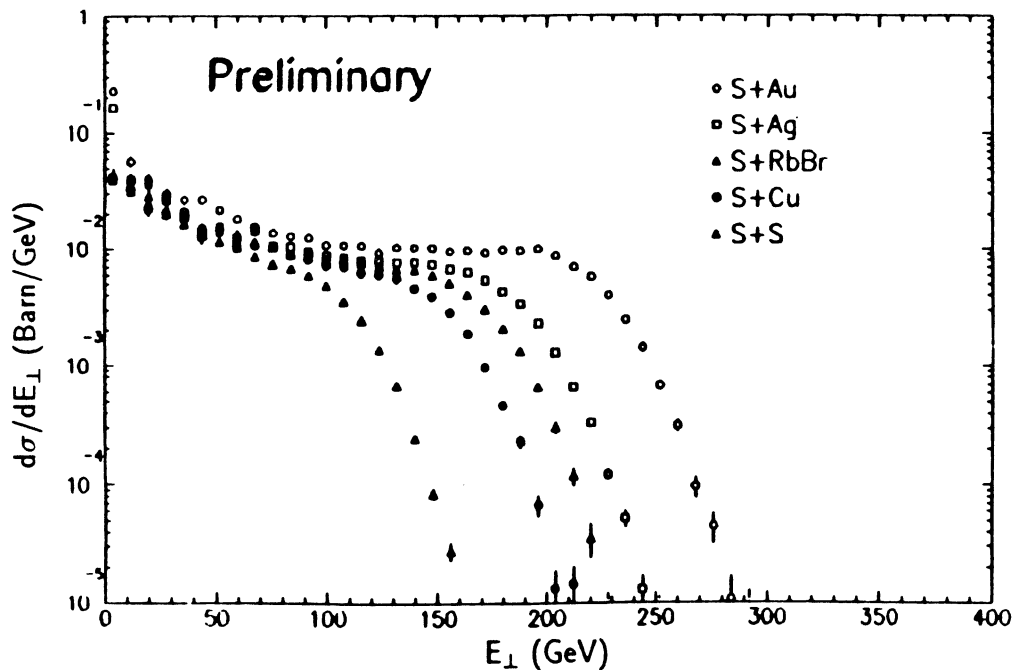

Figure 2. Transverse energy distributions for reactions of 200 GeV/n S on various targets in the acceptance $2.2 < \eta < 3.6$ for a minimum bias trigger.

The degree of nuclear stopping can be estimated by considering the average transverse energy observed in central collisions. For 200 GeV/n O + Au and S + Au collisions the average $E_\perp$ of the central collision peak is $< E_\perp^{central} > = 100 \pm 10$ GeV and 205 ± 10 GeV, respectively, for the interval $2.2 \leq \eta \leq 3.6$. (Measuring on the tail of the $E_\perp$ distribution at one percent of the cross section we get $E_\perp^{tail} = 150 \pm 10$ GeV and 275 ± 10 GeV.) Values of $< E_\perp^{central} > \simeq$ 95 ± 15 GeV and 175 ± 15 GeV ($E_\perp^{tail} \simeq 170 \pm 10$ GeV and 270 ± 10 GeV) are observed by Na34 [6,7] for 200 GeV/n O + W and S + W in the interval $-0.1 \leq \eta \leq 2.9$. Assuming negligible difference between the Au and W targets and subtracting the transverse energy in the overlap region of the two acceptances (taken to be half of the observed NA35 transverse energy), a total of $< E_\perp^{central} > \simeq 145$ GeV and 275 GeV ($E_\perp^{tail} \simeq 245$ GeV and 405 GeV) transverse energy are observed for 200 GeV/n O + Au and S + Au, respectively, in the region $-0.1 \leq \eta \leq 3.6$. These

values correspond to 0.37 and 0.40 (0.63 and 0.59 on the tails) of $E_\perp^{max}$ for the O + Au and S + Au reactions for the interval $-0.1 \leq \eta \leq 3.6$. They are suggestive of a large degree of stopping at 200 GeV/n, although the stopping is incomplete. It should be emphasized that for light projectiles incident on heavy targets, the transverse energy distributions are dominated by the geometry of the collisions. This has enabled the experiments to utilise calorimetry to trigger efficiently on the centrality of events.
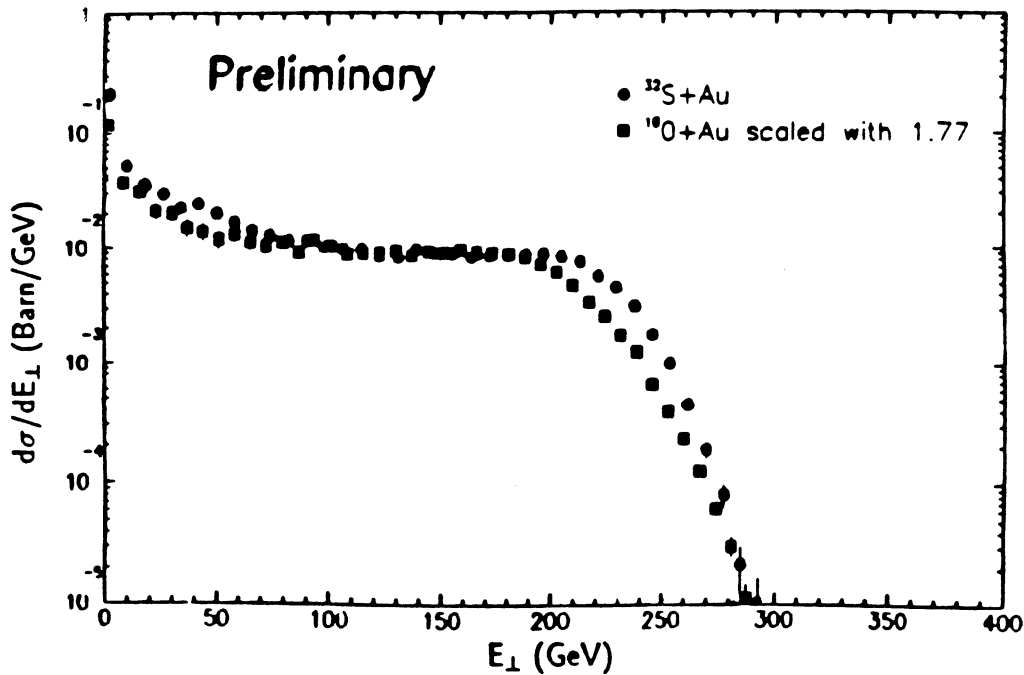

Figure 3. Transverse energy distributions for the reactions of S + Au and O + Au at 200 GeV/n in the acceptance $2.2 < \eta < 3.6$ for a minimum bias trigger. The $E_\perp$ axis for O + Au is scaled up by a factor 1.77.

4. PARTICLE PRODUCTION

4.1. Rapidity and Transverse Momentum Distributions

The rapidity distribution of negatively-charged particles in 200 GeV/n S + S collisions is displayed in Fig. 4 assuming the particles are pions. An approximate ten percent contamination of this sample by kaons is expected. Only the region $y < 3$ is displayed, since measurements in the forward region $\theta_{lab} < 2.3°$ are strongly affected by losses due to the high particle track density. Because of the projectile-target symmetry of the S + S system the rapidity distribution is, on the average, reflection symmetric about $y_{cm} = 3$. The rapidity distribution peaks at midrapidity with approximately 30 negatively-charged particles per unit rapidity. The width of the distribution $\Delta y_{fwhm} = 3.2$ is narrower than that observed for minimum bias 200 GeV p + p interactions ($\Delta y_{fwhm} = 3.5$)[8] but broader than that for emission from an isotropic fireball of temperature T > 100 MeV ($\Delta y_{fwhm} \simeq 1.8$). This is consistent with the geometrical picture of partial stopping observed in the $E_\perp$ distributions. A study[9] of the cross sections and multiplicity distributions of charged

particles for 60 and 200 GeV/nucleon ^{16}O projectiles by the NA35 collaboration has shown that the interaction cross sections follow a geometrical dependence on the nuclear radii and the multiplicity distributions are approximately consistent with a convolution of nucleon-nucleus collisions.

The mean transverse momentum $< p_\perp >$ of produced particles has been proposed[10] as a measure of the temperature[11] of the system. A complication in this proposition is that the temperatures reflected in the $p_\perp$ spectra for hadrons correspond to the temperature of the freezeout stage of the reaction, after hadronization, expansion and cooling. In fact, the $p_\perp$ distributions at midrapidity of negatively-charged particles from 200 GeV/n ^{16}O + Au central interactions cannot be fitted with a thermal distribution assuming a single temperature $(\chi^2/N = 5.2)$.[12,13] A single temperature fit assuming the negatively-charged particles are pions in a thermal Bose-Einstein distribution can reproduce the minimum bias 200 GeV p + p data at midrapidity. The temperature T = 135 ± 2 MeV fits those data well $(\chi^2/N = 2.2)$, with only slight deviations at $p_\perp < 0.1$ GeV and $p_\perp > 1.0$ GeV. [12] However, a two-temperature fireball parameterization is required to fit the 200 GeV/n ^{16}O + Au spectra.[12,13] The two components are $T_1 = 153 \pm 5$ MeV and $T_2 = 43 \pm 6$ MeV, with relative contributions $N_2/N_1 = 0.23 \pm 0.07$ and $\chi^2/N = 1.8$.
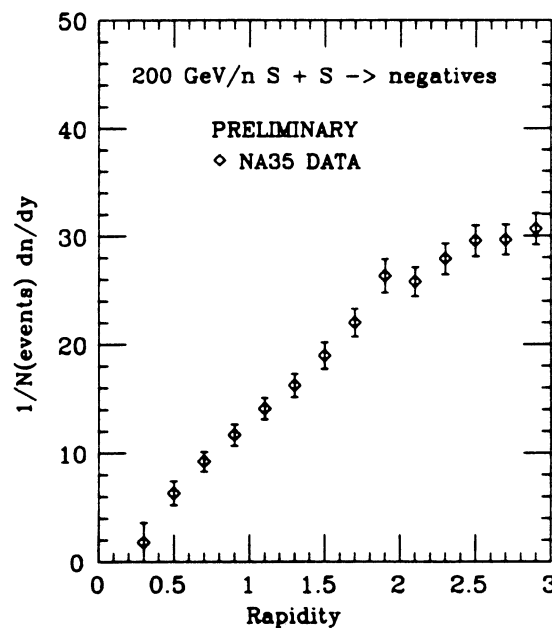

Figure 4. Rapidity distribution of negatively-charged particles in central S + S interactions at 200 GeV/n. Only $y < y_{cm}$ is displayed for the symmetric S + S reaction.

Perhaps a more realistic parameterization is that of a radially expanding fireball assuming an initial state in thermal equilibrium at fixed temperature with subsequent hydrodynamic expansion characterised by a radial flow velocity $\beta(r) = (r/R_0)^n \beta_s$. The exponent n is a parameter which categorizes the type of expansion and is fit to the data, r is the distance of the particle from the center of the system, and β_s is the particle velocity at the surface of freezeout radius R_0. This formulation is a generalization of the model of Ref. 14 where n = 1 was assumed for the expansion dynamics. A model with n ≠ 1 was introduced in Ref. 15 to investigate shapes of pion spectra. The authors of Ref. 16 found that the n = 2 parameterization of the expansion fit well the $p_\perp$

distribution of π^0 from WA80 [17] and the π^- distributions of the present experiment. If we fix n = 2 and $\beta_s = 0.78$, which are the values of Ref. 16 , and fit the negatively-charged particle data assuming pions, then a good fit ($\chi^2/N = 1.56$) is obtained with T = 108 MeV. A similar value of T was obtained in Ref. 16. The central 200 GeV/n O + Au data on negatively-charged particles and the radial expansion fit are displayed in Fig 5a. The data rise above the fit for $p_\perp < 0.1$ GeV/c. Displayed in Figs. 5b,c and d are the $p_\perp$ distributions for K^0, Λ and $\bar{\Lambda}$ measured in the streamer chamber[18] in central 200 GeV/n O + Au interactions. Superimposed are predictions for the spectra using the values n = 2, $\beta_s = 0.78$ and T = 108 MeV which best fit the pion data. The calculation for a radially expanding fireball is consistent with the $p_\perp$ distribution for K^0's and $\bar{\Lambda}$'s, but the prediction for the $p_\perp$ distribution of Λ's has a slightly flatter slope than the data. It appears that the model fairly successfully predicts the $p_\perp$ distributions for the produced particles (π's, K^0's and $\bar{\Lambda}$'s) while it has difficulties describing the Λ spectrum. Since the Λ will most easily be formed from a valence (ud) di-quark and a produced s quark, its spectrum may still have a nonthermal component due to the (ud) di-quark. The π's, K^0's and $\bar{\Lambda}$'s will be less influenced by dynamics of the incident channel. In addition, subtle dynamical effects in the evolution of the expanding system for the various produced particles, particularly the strange particles,[19] can alter their spectra.

The $p_\perp$ distribution for negatively-charged particles at $2 < y < 3$ in the 200 GeV/n S + S system is displayed in Fig. 6a. This distribution is identical, within statistical errors, to that of the 200 GeV/n O + Au data displayed in Fig. 5a. This strongly suggests that the observed particles, near midrapidity, are not affected by the spectator matter inherently present in the O + Au reaction. A radial expansion with parameters fitted to Fig. 5a is also displayed in Fig. 6a for comparison. Displayed in Fig. 6b is the $p_\perp$ distribution of the difference of positively- and negatively-charged particles near midrapidity, calculated on the assumption that the difference is due to protons. The errors are large because the distribution is derived from the small difference of large numbers. This distribution corresponds to the final distribution of the original ("primordial") proton charge in the collision. Predictions of the radial expansion model are superimposed on the pion data in Fig.6a. As in the case of the $p_\perp$ distribution of Λ's, the radial expansion model predicts a slightly flatter slope for the "proton" data than observed. This suggests that the incident charge is not completely equilibrated in the collision, although better statistics are necessary to solidify this hypothesis.

The general features of the $p_\perp$ distributions for the produced particles are surprisingly well reproduced by the model. However, details of the spectra, although reproduced by this simple model, may actually have more complicated origins. Displayed in Figs. 7a and b are ratios $R_{O(p)}(p_\perp) \equiv (O(p) + Au)^{negatives}_{central}/(p + p)^{negatives}_{min.bias}$ of O + Au and p + Au data with respect to minimum bias p + p data[20] as a function of $p_\perp$. An enhancement at low and high $p_\perp$, i.e. $p_\perp < 0.2$ GeV/c and $p_\perp > 1.0$ GeV/c, is observed in both systems. The $p_\perp$ distribution for p + Au in central collisions exhibits effects which must have similar origin and interpretations as in the O + Au data. This effect in the ratios plotted in Figs. 7a and b has also been observed in

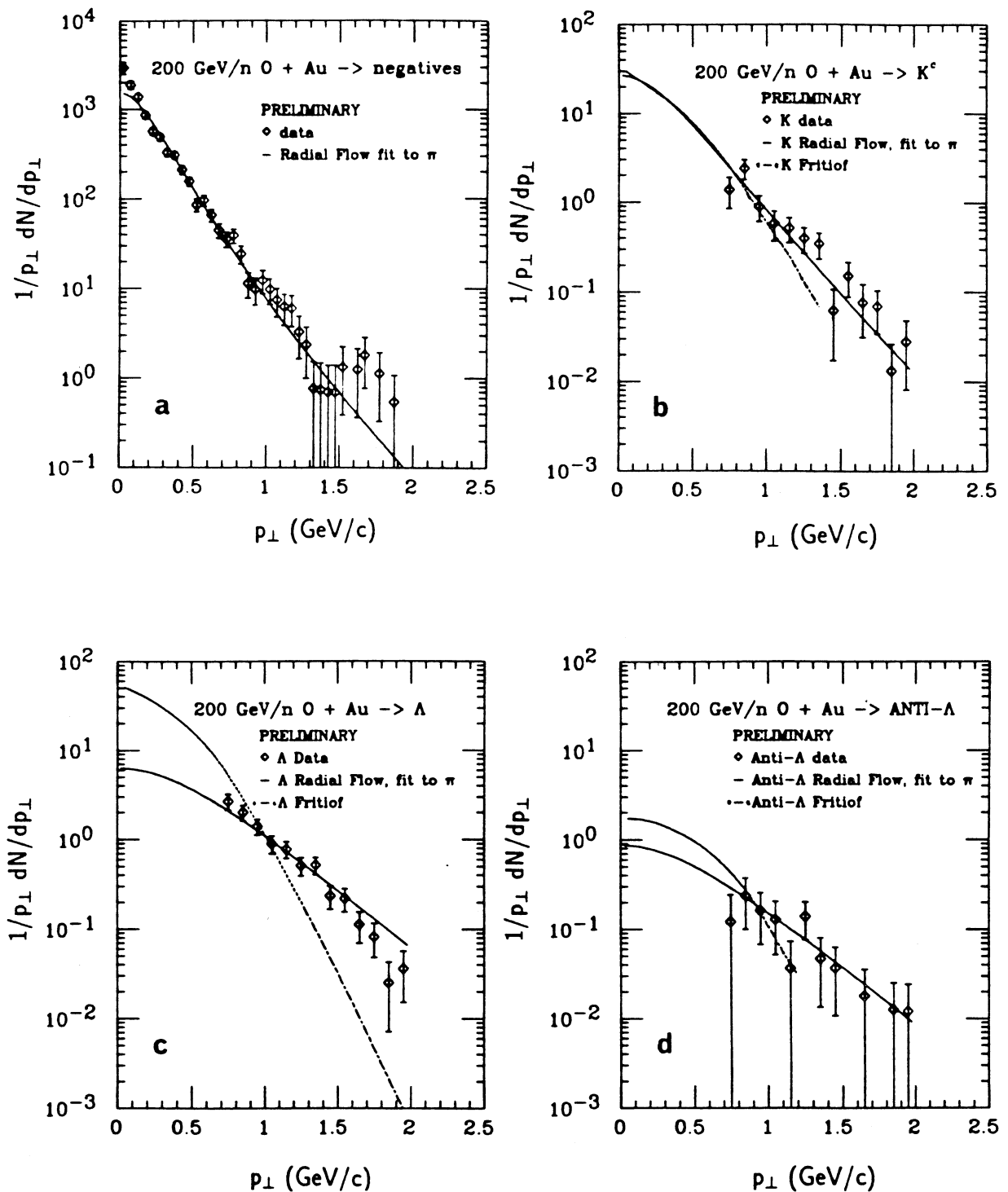Figure 5. Transverse momentum distributions for central collisions of 200 GeV/n O + Au for a) negatively-charged particles (2 < y < 3), b) K⁰'s (1.7 < y < 2.8), c) Λ's (1.5 < y < 2.4), and d) Λ̄'s (1.5 < y < 2.4). Also shown are predictions of a radial expansion model (solid curve) fitted to the distribution of negatives in a) and the Lund/Fritiof model (dot-dash curve) as described in the text.

very high charged-particle multiplicity (N_{ch}) p + p and $\alpha + \alpha$ events at $\sqrt{S}_{NN} = 63$ and 31.2 GeV, respectively.[21] These ratios relative to minimum bias data are plotted in Figs. 8a and b for intermediate ($6 \le N_{ch} \le 10$) and high ($N_{ch} \ge 18$) multiplicity events. The enhancements at low and high $p_\perp$ are not observed in the low and intermediate multiplicity data. The structure of the ratios for $N_{ch} \ge 18$ events are remarkably similar to those of the central p + Au and O + Au data in Figs. 7a and b. The marked similarity of central p + Au and O + Au collisions to very high multiplicity "hard-scattering" p + p and $\alpha + \alpha$ collisions suggests an explanation may need to be found at the quark-parton level.
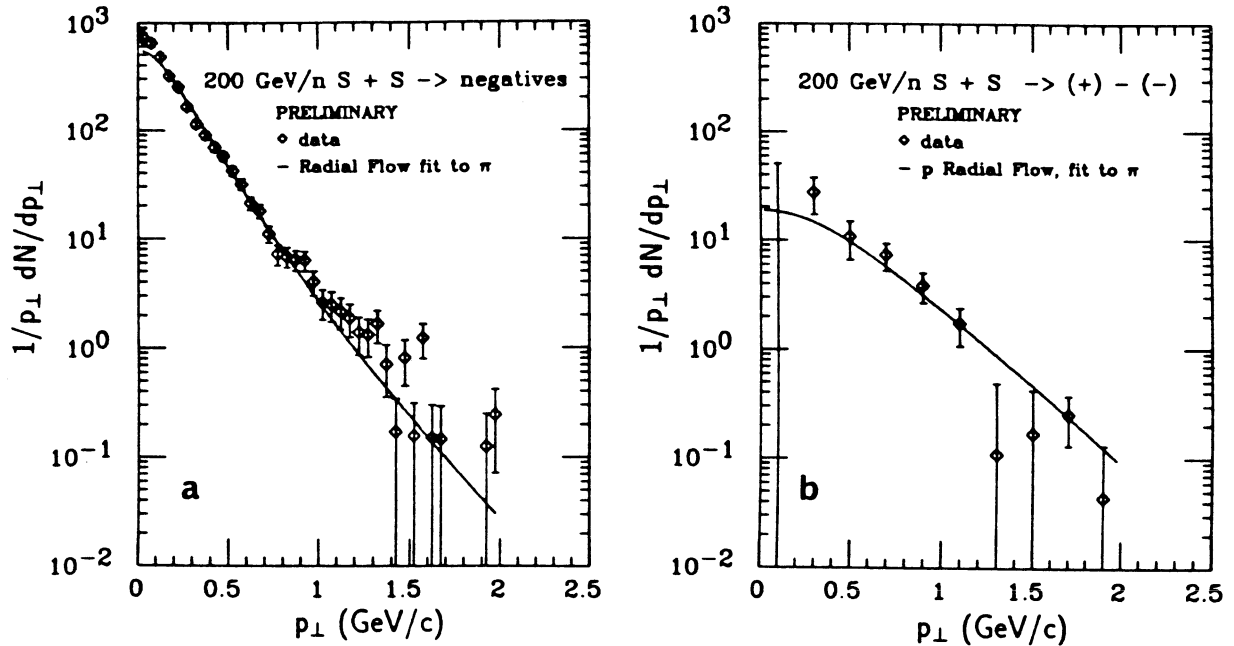

Figure 6. Transverse momentum distributions for central collisions of 200 GeV/n S + S for a) negatively-charged particles ($2 < y < 3$) and b) the difference of positively- and negatively-charged particles assuming they are protons. Also shown are predictions of a radial expansion model fitted to the distribution of negatives in Fig. 5a as described in the text.

4.2. Two-Pion Interferometry

Hanbury Brown and Twiss (HBT) correlations[22] between negatively-charged pions have been measured by NA35 in the 200 GeV/n O + Au reaction and the results published.[23] A summary of the results are listed in Table 1. The approach involves a Gaussian parameterization[24] of the pion-emitting source with R_T the transverse radius, R_L the longitudinal radius and Λ the chaoticity parameter. Also listed are results of fits using another parameterization[25] of the source distribution which is Lorentz-covariant and incorporates the inside-outside cascade for the collision dynamics. The parameters in this model are the source lifetime τ_0, R_T and Λ. A value of $\Lambda = 1$ corresponds to chaotic emission from the source. Values of $\Lambda < 1$ correspond to decreasing chaoticity, with $\Lambda = 0$ total coherence. As observed in Table 1 pions at $2 < y < 3$ near midrapidity in the effective ^{16}O + Au center-of-mass ($y_{cm} = 2.5$) originate from a large ($R_T \simeq 8$ fm), relatively chaotic ($\Lambda \simeq 0.8$), long-lived ($\tau_0 = 6.4$ fm/c) source. This picture suggests the formation of a thermalised fireball at midrapidity. These conditions are necessary for the possible formation of a quark-gluon plasma. In fact, considering the large number of produced particles, mostly pions, near midrapidity
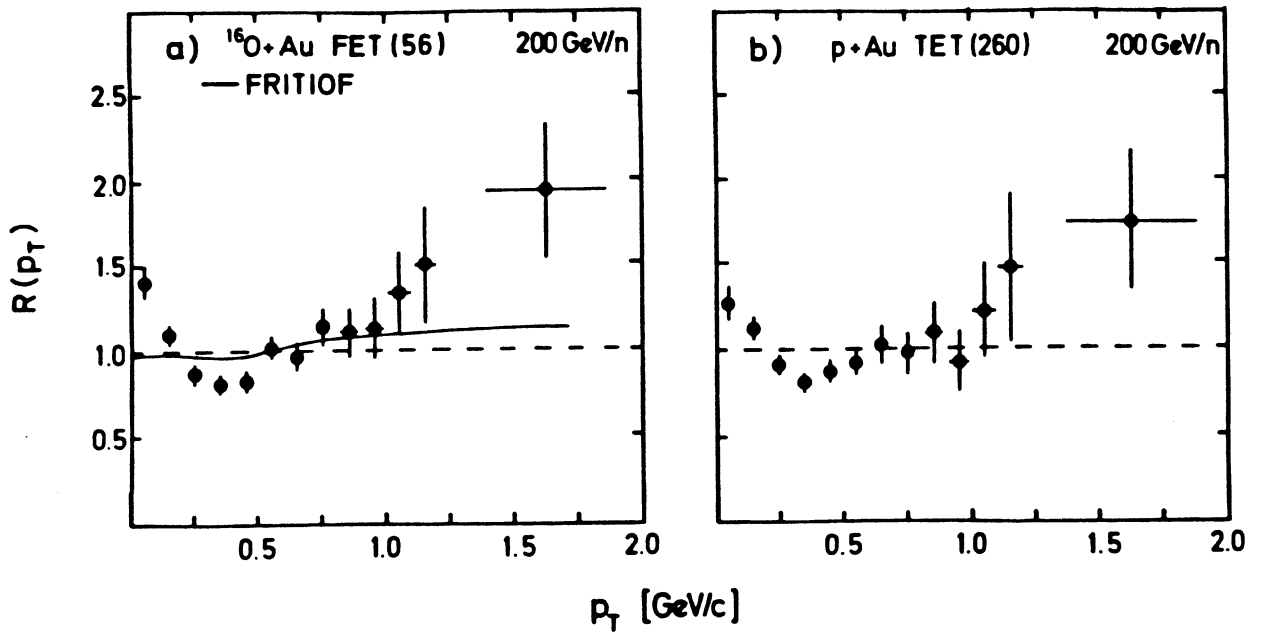
Figure 7. Ratios $R(p_T)$ of the transverse momentum distributions of central a) ^{16}O + Au and b) p + Au collisions relative to minimum bias p + p collisions at 200 GeV/n. The dashed lines indicate $R(p_T) = 1$. The trigger conditions were a) "forward energy trigger" FET(56) and b) "transverse energy trigger" TET(260) with trigger cross sections of 56 and 260 mb, respectively.

Figure 8. Ratios $R(p_T)$ of the transverse momentum distributions of selected charge multiplicity (N_{ch}) p + p and $\alpha + \alpha$ events at $\sqrt{S}_{NN}$ = 63 and 31.2 GeV, respectively, relative to minimum bias data for a) intermediate $(6 \leq N_{ch} \leq 10)$ and b) high $(N_{ch} \geq 18)$ multiplicity events from Ref. 21.

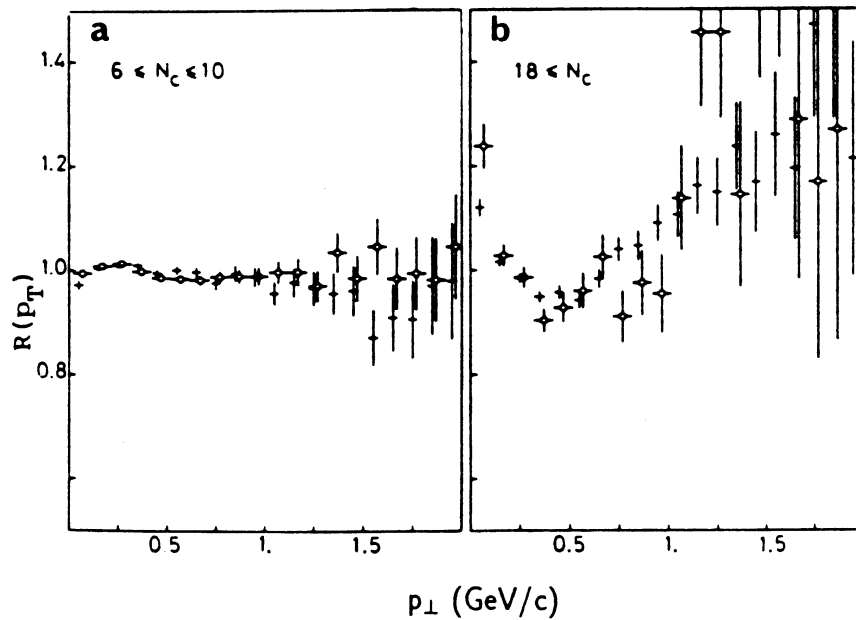in central collisions of O + Au at 200 GeV/n (approximately 120 - 140 per unit rapidity[12,23]) and the $\pi\pi$ strong interaction cross sections, one predicts a similar size (R $\simeq$ 8 fm) for the system of pions at the time of their last interaction (freezeout). Preliminary results on HBT correlations for negatively-charged pions from central 200 GeV/n S + S collisions are displayed in Table 2 assuming a static Gaussian source. The same effect of a large source of midrapidity pions, in this case y_{cm} = 3, is again observed. The errors are still fairly large due to the small data set presently analysed.

Table 1. Pion source parameters extracted from analysis of the 200 GeV/n O + Au $\rightarrow$ $\pi\pi$ correlation data for various rapidity intervals.

Rapidity Interval	Gaussian			Kolehmainen-Gyulassy		
	R_T(fm)	R_L(fm)	Λ	R_T(fm)	τ_0(fm/c)	Λ
1 < y < 4	4.1 ± 0.4	3.1 +0.7/-0.4	0.31 +0.07/-0.03	3.6 ± 0.3	2.9 ± 0.7	0.29 ± 0.05
1 < y < 2	4.3 ± 0.6	2.6 ± 0.6	0.34 +0.09/-0.06	4.0 ± 0.7	2.5 ± 1.0	0.30 ± 0.12
2 < y < 3	8.1 ± 1.6	5.6 +1.2/-0.8	0.77 ± 0.19	7.3 ± 1.6	6.4 ± 1.0	0.84 ± 0.15

Table 2. Pion source parameters extracted from analysis of the 200 GeV/n S + S $\rightarrow$ $\pi\pi$ correlation data for various rapidity intervals.

Rapidity Interval	Gaussian		
	R_T(fm)	R_L(fm)	Λ
1.5 < y < 4.5	5.6 ± 0.8	3.1 ± 0.3	0.47 ± 0.15
1.5 < y < 2.5	6.2 ± 1.2	1.7 ± 0.8	0.57 ± 0.17
2.5 < y < 3.5	8.7 ± 2.7	3.6 ± 2.0	0.68 ± 0.25

Pions over the larger rapidity range reflect a much smaller source ($R_L \simeq$ 3 fm), with much less chaoticity. Away from midrapidity the transverse size is near that of the incident projectile, the longitudinal size is small and the chaoticity parameter is low, near that of e^+e^- and hadron-hadron collisions. The observation $R_L < R_T$ for all rapidity intervals studied is a result of the pion coherence length and the effect of relativistic kinematics.[26] R_L is less than R_T because of the Lorentz contraction of R_L away from y_{cm} whereas R_T is unaffected. Furthermore, after unfolding the kinematics R_L can be used to determine the correlation length $\Delta y \approx 1$. It has been suggested[26] that the correlation length in momentum space is related to the QCD string tension. Further investigation is necessary to determine the correlation length and ultimately the QCD string tension in high energy nucleus-nucleus collisions where large numbers of overlapping strings are expected.

A suggestion was recently made[27,28] to analyse the $\pi\pi$ correlation in the cm frame in terms of the two orthogonal directions transverse to the beam, labelled "outward" (along the direction of one of the pions or the momentum vector sum transverse to the beam) and "sideward" (perpendicular to the beam and the outward direction). A measure of the transverse size along the outward direction will reflect any prolonged emission or long-lived state such as a quark-gluon plasma state. The 200 GeV/n O + Au central collision data analysed in Table 1, have been analysed in these parameters near midrapidity (2 < y < 3) and away from midrapidity (1 < y < 2). The results are displayed in Table 3. The R_L and Λ parameters were held constant at the best-fit values of Table

1 and the R_T subdivided into R_T^{out} and R_T^{side} and both allowed to vary. Away from midrapidity we find that $R_T^{out} = R_T^{side}$, whereas near midrapidity $R_T^{out} = 11.2 \pm 2.3$ fm and $R_T^{side} = 6.6 \pm 1.8$ fm. According to Refs. 27 and 28 these data suggest a long-lived state which prolongs the outward emission reflecting a larger outward than sideward size in the midrapidity region. Away from midrapidity the two sizes are the same as would be expected for a hadron gas. A recent paper[29] has investigated further the sensitivity of the outward and sideward analysis of $\pi\pi$ interferometry. They conclude that the results described in Tables 1,2,3 are consistent with a range of pion source parameters for a hadron gas when additional dynamical effects including higher resonances are included in the analysis. It appears that the spacetime evolution of these collisions is quite complicated with possible phase changes and subsequent hadronisation and should be a source of much future interest and debate.

Table 3. Pion source parameters extracted from analysis of the 200 GeV/n O + Au $\to \pi\pi$ correlation data with separation of R_T into R_T^{side} and R_T^{out} as suggested in Refs. 27 and 28. Rapidity intervals at midrapidity $(2 < y < 3)$ and backward of midrapidity $(1 < y < 2)$ were analysed.

Rapidity Interval	Gaussian		
	R_T(fm)	R_L(fm)	Λ
$1 < y < 2$	4.3 ± 0.6	2.6 ± 0.6	$0.34 +0.09/-0.06$
	$R_T^{side} = 4.0 \pm 1.0$ fm	"	"
	$R_T^{out} = 4.4 \pm 1.0$ fm	"	"
$2 < y < 3$	8.1 ± 1.6	$5.6 +1.2/-0.8$	0.77 ± 0.19
	$R_T^{side} = 6.6 \pm 1.8$ fm	"	"
	$R_T^{out} = 11.2 \pm 2.3$ fm	"	"

4.3. Neutral Strange Particle Production

One of the earliest predictions for a signature of the deconfinement transition was an enhancement of s and $\bar{s}$ quarks in a quark-gluon plasma in thermal and chemical equilibrium.[30] Most calculations predict an enhancement in the observed $\bar{s}$ yield as a signature of plasma formation while s quark yields, although enhanced, differ only slightly in a plasma compared to a hadron gas. It has recently been noted[31] that the actual observation of $\bar{s}$ enhancement after plasma formation is severely complicated by the spacetime evolution of the collision process, making it difficult to discriminate between the hadronisation products of a quark-gluon plasma and those of a chemically-equilibrated hadron gas. However, it is highly unlikely that hadronic processes in the nonplasma phase are best represented by an equilibrium hadron gas. In any case the dynamics complicate the issue and both the reaction dynamics and the strange particle abundances must be understood.

The streamer chamber can be used to identify the decays of neutral strange particles into charged particles. The decay vertex is identified in the streamer chamber and the momenta of the positively- and negatively-charged products are measured. Assuming masses corresponding to the decays $K^0 \to \pi^+\pi^-$, $\Lambda \to p\pi^-$, $\bar{\Lambda} \to \pi^+\bar{p}$ and applying kinematic fitting criteria, unambiguous K^0, Λ, $\bar{\Lambda}$ decays are identified and the strange particle momenta determined. Efficiency corrections are

applied for obscuration of the decay vertex, problems of identification, measuring and reconstruction inefficiencies and the finite chamber geometry. Displayed in Fig. 9a,b and c are ratios of the number of strange particles $(K^0, \Lambda, \bar{\Lambda})$ to the number of negatively-charged particles for 60 and 200 GeV/n O + Au, and 200 GeV p + Au in the acceptances measured in the NA35 experiment. This acceptance corresponds to fairly high $p_\perp$, $p_\perp > 0.7$ GeV/c, near midrapidity. The rapidity ranges are given in Fig. 9. The events were selected by triggering with external calorimeters on trigger cross sections of 1.14, 0.24 and 0.13 barns for the reactions 200 GeV p + Au, 200 GeV/n O + Au and 60 GeV/n O + Au, respectively. These correspond to 0.67, 0.07 and 0.04 of the total inelastic cross sections for those reactions. Also shown are ratios for 205 and 360 GeV p + p from Refs. 32 and 33 and 200 GeV p + Au from NA35 measured over larger acceptances, $p_\perp > 0.1$ GeV/c and rapidities stated in Fig. 9. At 200 GeV/n the p + Au ratios are identical to those of O + Au measured over the same acceptance. Predictions of the Lund/Fritiof model[34] taken over these acceptances are in agreement with all the data for K^0's and the high $p_\perp$ $\bar{\Lambda}$-data for p + Au and O + Au. However, the Lund/Fritiof model underpredicts by approximately a factor of 2 the high $p_\perp$ Λ-data. More importantly, the Lund/Fritiof model appears to overpredict the Λ and $\bar{\Lambda}$ production in the elementary p + p reaction.
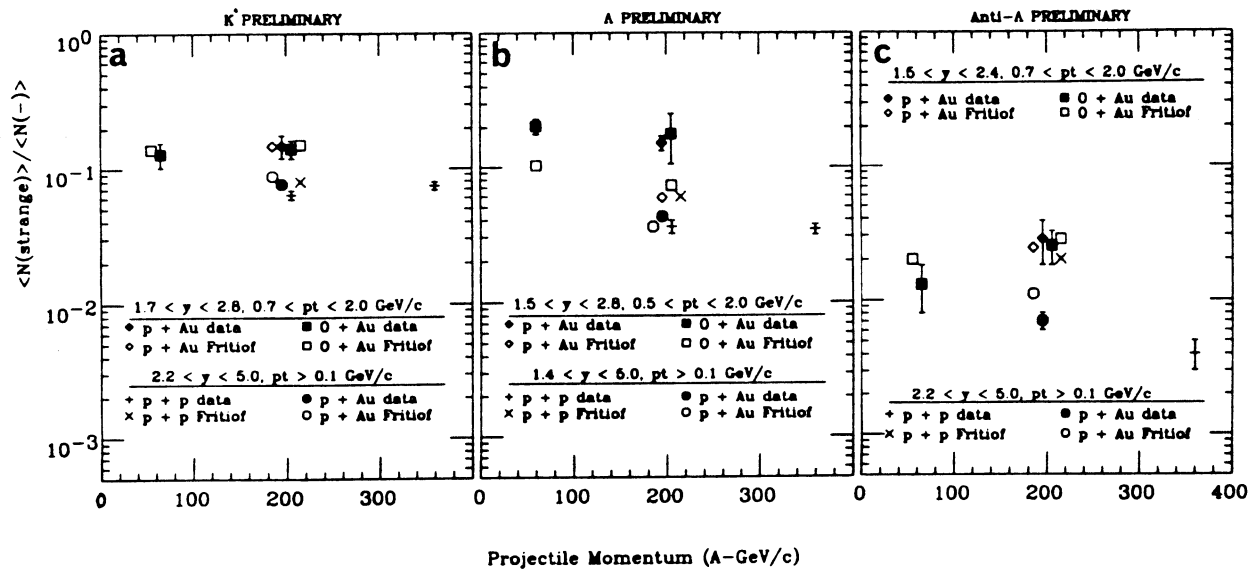

Figure 9. Ratios of the mean numbers of strange particles a) $<N(K^0)>$, b) $<N(\Lambda)>$ and c) $<N(\bar{\Lambda})>$ to the mean number of negatively-charged particles $<N(-)>$ as a function of incident beam momentum.

The ratios displayed in Fig. 9 are very much dependent upon the $p_\perp$ region over which they are accumulated. Displayed in Fig. 5 along with the $p_\perp$ distributions of K^0's, Λ's and $\bar{\Lambda}$'s for 200 GeV/n O + Au are predictions of the Lund/Fritiof model. The model underpredicts the slopes of the K^0, Λ and $\bar{\Lambda}$ data. It's obvious from Fig. 5 that comparisons such as particle ratios or ratios of experiment to theory will be strongly influenced by the region of $p_\perp$ under consideration. With the exception of the large acceptance p + p and p + Au data, the discrepancies observed in Fig.

9 can be understood from the difference in the slopes of the $p_\perp$ spectra. The data in Fig. 5 can also be fitted with $(1/p_\perp)d\sigma/dp_\perp = Ae^{-Bm_\perp}$ where A is a normalization parameter, B represents the inverse slope of the spectrum and $m_\perp = \sqrt{m^2 + p_\perp^2}$ denotes the transverse mass. The best-fit values of the slopes of the spectra are listed in Table 4. These values are similar within errors for the K^0, Λ, and $\bar{\Lambda}$ data measured in the 60 and 200 GeV/n O + Au and 200 GeV p + Au interactions.

Table 4. Slope parameters B derived from fits of the form $(1/p_\perp)d\sigma/dp_\perp = Ae^{-Bm_\perp}$ to the transverse momentum distributions for $p_\perp > 0.7$ GeV/c. The $m_\perp = \sqrt{m^2 + p_\perp^2}$ is the transverse mass.

	200 GeV/n p + Au	200 GeV/n O + Au	60 GeV/n O + Au
K^0	4.9 ± 0.4	4.2 ± 0.4	4.6 ± 0.7
Λ	4.7 ± 0.5	4.9 ± 0.3	4.7 ± 0.4
$\bar{\Lambda}$	5.8 ± 0.7	3.2 ± 1.4	5.8 ± 1.3

The ratios of the multiplicities of K^0, Λ, $\bar{\Lambda}$ and all negatively-charged particles for O + Au relative to p + Au measured at 200 GeV/n are listed in Table 5. These ratios are close to the value 16, which is the ratio of the numbers of incident projectile nucleons. Since the triggers correspond to very central O + Au (where most of the incident nucleons of the O projectile would be expected to interact) and relatively inelastic p + Au interactions, it appears that a super-position of 16 p + Au interactions reproduces the observed O + Au particle multiplicities This was also the case for the $E_\perp$ distributions[3], cross sections and shapes of charged particle multiplicity distributions.[9] Detailed calculation of the ratios in Table 5 will have to include, among other geometrical constraints, subtle effects of the difference in the center-of-mass and the various penetration depths seen by incident nucleons at impact parameters constrained by the two triggers.

Table 5. Ratios of K^0, Λ, $\bar{\Lambda}$ and negatively-charged particle multiplicities measured in central O + Au relative to inelastic p + Au reactions at 200 GeV/n. The ratios are for the high $p_\perp$ acceptance regions in Fig. 9. Also shown are predictions of the Lund/Fritiof model.

	200 GeV/n Data	200 GeV/n Fritiof
$< N_{K^0} >_{O+Au} / < N_{K^0} >_{p+Au}$	15.1 ± 3.4	16.5 ± 0.8
$< N_\Lambda >_{O+Au} / < N_\Lambda >_{p+Au}$	18.6 ± 2.5	20.1 ± 2.1
$< N_{\bar{\Lambda}} >_{O+Au} / < N_{\bar{\Lambda}} >_{p+Au}$	16.3 ± 7.0	18.4 ± 3.8
$< N_- >_{O+Au} / < N_- >_{p+Au}$	15.9 ± 1.2	16.2 ± 0.3

Neutral strange particle production in 200 GeV/n S + S interactions has been analysed to provide information on the volume dependence of strangeness production. The yields of K^0's and Λ's as a function of event centrality are displayed in Fig. 10. Plotted are the mean numbers of K^0's and Λ's as a function of the mean charged particle multiplicity in the event sample. Details of the analysis can be found in Ref. 35. Increasing multiplicities of charged particles correspond to smaller impact parameters in a geometrical model. Little spectator matter is expected to remain in central collisions of S + S, in differentiation to collisions of O + Au. The Λ yield rises as a

function of event centrality to a value more than twice that expected from the Lund/Fritiof model or an independent nucleon-nucleon model extrapolated from p + p to the S + S case.[35] The K^0 yield also rises above predictions but to a lesser degree than the Λ's. The dependence of $<N(\lambda)>$ on $<N(+-)>$ is steeper than linear, i.e. $<N(\lambda)> \sim <N(+-)>^{\alpha}$ where $\alpha > 1$. Also plotted in Fig. 10 are predictions of a simple hadron gas model (double line), which lies near the Lund/Fritiof and nucleon-nucleon model predictions, and a parton gas model (triple line) which predicts enhanced yields[35] near those observed.
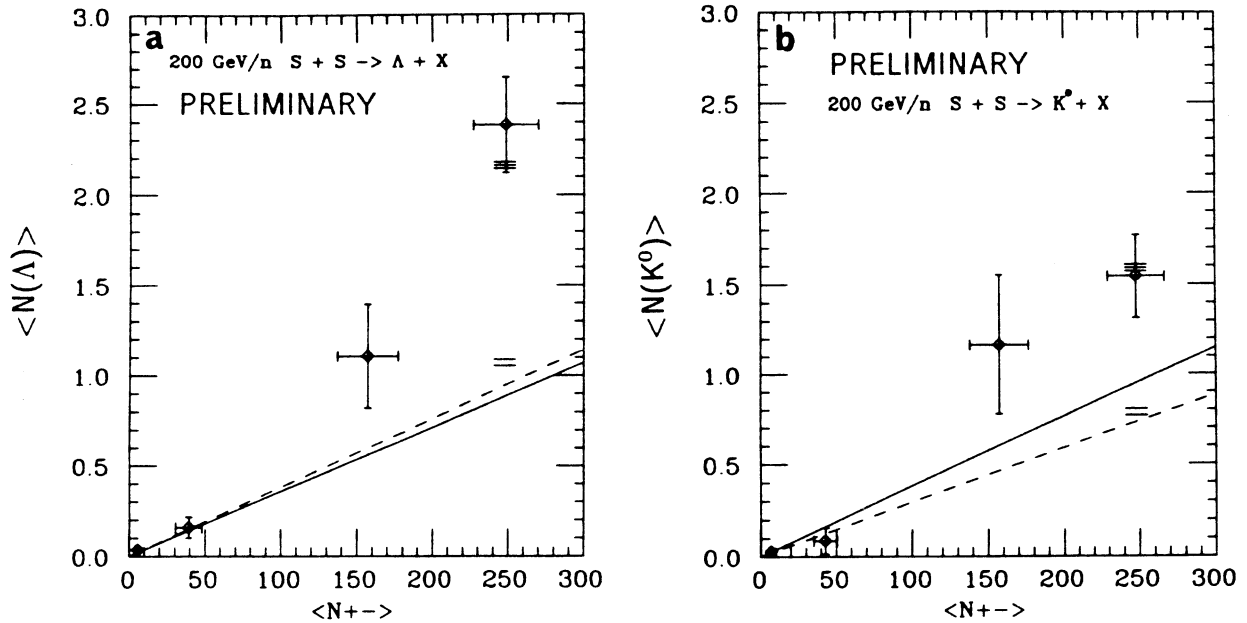

Figure 10. For 200 GeV/n S + S interactions, the mean multiplicities of a) Λ's and b) K^0's as a function of the mean charged particle multiplicity in each event sample. The solid lines are predictions of the Lund/Fritiof model and the dashed lines those of an independent nucleon-nucleon model. The double line is the prediction of a hadron gas model for central collisions and the triple line that for a parton gas (see Ref. 35).

5. CONCLUSIONS

Most of the data presented on transverse energy distributions, forward energy flow, mean particle multiplicities, interaction cross sections and rapidity distributions provide information which can be interpreted by a geometrical folding of nucleon-nucleus interactions in a nucleus-nucleus collision geometry. The stopping is incomplete at 200 GeV/n, but at least 40 percent of the maximum available transverse energy is observed in average central O + Au and S + Au collisions and at least 60 percent for collisions with a cross section of one percent of that of the average central collision. The resultant nucleus-nucleus interactions appear to have sufficient stopping to produce energy densities $\epsilon \approx$ 2-3 GeV/fm^3 in the tails of the distributions. From geometrical considerations and the scaling observed in the experiment, the transverse energy of average central collisions scales as $E_\perp \sim A_{proj}$ for $A_{proj} < A_{target}$. The volume V scales as $V \sim A_{proj}^{2/3} A_{target}^{1/3}$. Therefore, the energy density $\epsilon = E_\perp / V \sim A_{proj}^{1/3}$. In extrapolating from the measured S + Au transverse energy distributions by use of the $A_{proj}^{1/3}$ scaling for ϵ, the energy densities for Pb + Pb

are expected to increase by approximately a factor of 1.8 - 1.9 and the volume by 3 - 4 over present values for S + Au.

A large number of produced particles, mostly pions, is observed at midrapidity in 200 GeV/n O and S induced interactions. These are strongly peaked at midrapidity in the rest frame of geometrical overlap of the nucleus-nucleus collision. Estimating from the observed charged particle multiplicities, approximately 90 - 100 charged and neutral particles per unit rapidity for S + S and 120 - 140 particles per unit rapidity for O + Au exist in the final state at midrapidity. The transverse momentum distributions of negatively-charged particles at midrapidity cannot be described in terms of a thermal distribution with a single temperature at midrapidity. A multiple temperature parameterisation fits the data. A thermal distribution with superimposed radial flow also fits the negatively-charged particle data. Predictions of the radial flow model are also consistent with the transverse momentum distributions of heavier produced particles measured in NA35. The large source sizes observed in the $\pi\pi$ interferometry data appear to be consistent with the freezeout conditions taking into consideration the large number of hadrons present in the system and the $\pi\pi$ mean-free-path. In addition, the source parameters determined from $\pi\pi$ interferometry, the measured $p_\perp$ distributions and the rapidity density of charged particles measured in NA35 can be used to constrain the freezeout conditions in the radial expansion model, resulting in an average energy density of 1 - 2 GeV/fm^3 for central O + Au collisions.[16] It should be emphasized that the transverse momentum distributions of negatively-charged particles in central collisions of O + Au and p + Au at 200 GeV/n have enhancements at $p_\perp < 0.1$ GeV/c and $p_\perp > 1.0$ GeV/c which are not present in minimum bias p + p data. These enhancements have been observed in very high multiplicity p + p and $\alpha + \alpha$ events at higher energies suggesting a possible common description in terms of the "hard" scattering of partons. A sufficient number of hard parton scatterings might occur in central nucleus-nucleus collisions to dissolve the structure of the incident nucleons, thereby satisfying a prerequisite for quark-gluon plasma formation.

Ratios of neutral strange particles to negatively-charged particles measured in NA35 are the same for p + Au and O + Au at 200 GeV/n. Furthermore, the strange particles and negatively-charged particles are a factor of 16 more abundant in central O + Au than inelastic p + Au. These results are entirely consistent with a description of central O + Au interactions in terms of 16 inelastic p + Au interactions. For 200 GeV/n S + S an enhancement of the Λ, and to a lesser degree, the K^0 multiplicity in central interactions relative to peripheral ones has been observed. This strong dependence of the strange particle multiplicities as a function of centrality is neither reproduced by the Lund/Fritiof model nor by a superposition of nucleon-nucleon interactions. A parton gas model appears to be successful in producing the multiplicities observed in the data. Further study of this interesting effect for the asymmetric O + Au system should aid in understanding strange particle production in the two different systems.

REFERENCES

1. A. Sandoval et al., Nucl. Phys, A461 (1987) 465c.
2. M.L. Tincknell et al., Opt. Eng. 26 (1987) 1067.
3. A. Bamberger et al., Phys. Lett. B184 (1987) 271.
4. W. Heck et al., Z. Phys. C38 (1988) 19.
5. P. Braun-Munzinger, Proceedings of this Conference.
6. B. Jacak, Proceedings of the 3rd Conference on the Intersections between Particle and Nuclear Physics, Rockport, ME, USA May 14-19, 1988, to be published by the American Institute of Physics.
7. J. Schukraft, Proceedings of this Conference.
8. C. de Marzo et al., Phys. Rev. D26 (1982) 1019.
9. A. Bamberger et al., Phys. Lett. B205 (1988) 583.
10. E.V. Shuryak and O.V. Zhirov, Phys Lett. B89 (1980) 253 and Phys. Lett. B171 (1986) 99.
11. K. Redlich and H. Satz, Phys. Rev. D33 (1986) 3747.
12. H. Ströbele et al., Z. Phys. C38 (1988) 89.
13. R. Renfordt et al., Proceedings of this Conference.
14. P.J. Siemens and J.O. Rasmussen, Phys. Rev. Lett. 42 (1979) 880.
15. D. Hahn and N.K. Glendenning, Phys. Rev. C37 (1988) 1053.
16. K.S. Lee and U. Heinz, U. Regensburg Preprint (1988).
17. R. Albrecht et al., Z. Phys. C38 (1988) 97.
18. Details of the neutral strange particle production data will be discussed in section 4.3 including discussion of the Lund/Fritiof predictions in Figs. 5b,c and d.
19. U. Heinz, K.S. Lee and M.J. Rhoades-Brown, Phys. Rev. Lett. 58 (1987) 2292.
20. The NA5 Collaboration, private communication.
21. W. Bell et al., Phys. Lett. 112B (1982) 271; A. Karabarbounis et al., Phys. Lett. 104B (1981) 75; A.L.S. Angelis et al., Phys. Lett. 116B (1982) 379.
22. R. Hanbury Brown and R.Q. Twiss, Nature 177 (1956) 27 and Nature 178 (1956) 1046.
23. A. Bamberger et al., Phys. Lett. B203 (1988) 320.
24. F.B. Yano and S.E. Koonin, Phys. Lett. B78 (1978) 556.
25. K. Kolehmainen and M. Gyulassy, Phys. Lett. B180 (1986) 203.
26. B. Andersson and W. Hofmann, Phys. Lett. B169 (1986) 364.
27. S. Pratt, Phys Rev. D33 (1986) 1314.
28. G. Bertsch, M. Gong and M. Tohyama, Phys. Rev. C37 (1988) 1896 and G. Bertsch MSU Preprint (1988).
29. M. Gyulassy and S. S. Padula, LBL Report LBL-26077 (1988).
30. R. Hagedorn and J. Rafelski, Phys. Lett. 97B (1980) 180.

31. K.S. Lee, M.J. Rhoades-Brown and U. Heinz, Stony Brook Preprint (1987).

32. K. Jaeger et al., Phys Rev. D11 (1975) 2405.

33. M Asai et al., Z. Phys. C27 (1985) 11.

34. B. Andersson et al., Nucl. Phys. B281 (1987) 289; Versions FRITIOF 1.6 and JETSET 6.2 were used with standard parameters and a strange quark suppression factor of 0.3.

35. M. Gazdzicki et al., Proceedings of this Conference.